Journal of ELECTRONIC MATERIALS, Vol. 47, No. 1, 2018
DOI: 10.1007/s11664-017-5835-8

Magnetically Separable Fe_2O_3/g-C_3N_4 Nanocomposites with Cocoon-Like Shape: Magnetic Properties and Photocatalytic Activities

XIAOJIA YU,[1] XIAOYU YANG,[1] and GUANG LI[1,2,3,4]

1.—School of Physics and Materials Science, Anhui University, Hefei 230601, China. 2.—Anhui Key Laboratory of Information Materials and Devices, Hefei 230601, China. 3.—e-mail: liguang1971@ahu.edu.cn. 4.—e-mail: liguang64@163.com

We report magnetically separable Fe_2O_3/g-C_3N_4 nanocomposites as a photocatalyst under visible-light irradiation in this study. The Fe_2O_3/g-C_3N_4 nanocomposites were synthesized through a two-step hydrothermal method. The Fe_2O_3 with cocoon-like shape was obviously dispersed on the surface of g-C_3N_4 with porous and layered nanostructure as seen from micrographs of the particles. Furthermore, the magnetic conversion of the samples was studied via vibrating sample magnetometer technology. It was found that the saturated magnetization Ms of the Fe_2O_3/g-C_3N_4 nanoparticles obviously decreased in the presence of g-C_3N_4, and the photocatalytic activity of the samples investigated by degrading Rhodamine B suggested that the Fe_2O_3/g-C_3N_4 photocatalyst was prior to the pure Fe_2O_3 and g-C_3N_4 samples. In addition, the magnetically separable ability of Fe_2O_3/g-C_3N_4 nanocomposites was efficiently exhibited by an external magnet.

Key words: Magnetically separable, cocoon-like, Fe_2O_3/g-C_3N_4 nanocomposites, magnetic property, photocatalytic activity

INTRODUCTION

In recent years, graphitic carbon nitride (g-C_3N_4), as a polymer-like semiconductor, has drawn widespread attention in its electronic and photoluminescence properties.[1,2] Due to its large unique surface area and good chemical stability, g-C_3N_4 has been applied to various hybrid photocatalysts. However, there are some drawbacks of g-C_3N_4, including high recombination rate of photogenerated electron–hole pairs and low photocatalytic activity.[3] In this case, several previous studies have addressed these issues with success via preparing hybrid photocatalysts, such as fabricating nanocomposites and doping with metal or nonmetal elements.[4–6] However, there is a limitation in photocatalysts of g-C_3N_4-based nanocomposites for photocatalysis because of the ready losses in the reaction process.[7] In addition, the photocatalysts may easily precipitate from the aqueous solvent for degradation of Rhodamine B due to the poor control over the particle sizes and their distribution.[8] Therefore, in this study, we explored a facile but efficient synthesis route to prepare homogeneous nanocomposites.

Fe_2O_3 has been widely investigated in some fields of magnetism and photocatalyst due to its excellent photoelectronic properties, remarkable chemical stability, nontoxicity and low cost.[9–11] In addition, as a semiconductor with narrow band-gap energy under ambient conditions, Fe_2O_3 has widely been used to prepare visible-light-driven photocatalysts because of its visible-light absorbing capacity. Nevertheless, it has been found that single Fe_2O_3 normally shows low photocatalytic activity due to its rapid recombination rate of separated electron–hole pairs.[12,13] There are some strategies to solve this problem. One of which is to prepare composite photocatalysts with other semiconductors to benefit the capability of utilizing light, which promotes the visible-light absorbing ability.[14] Also, the

(Received May 17, 2017; accepted September 27, 2017; published online October 12, 2017)

combination of different energy levels from different semiconductors can develop a new system to create charge separation and reduce the recombination of photo-induced charge carriers.[15] In addition, the combination of Fe_2O_3 with graphene material exhibits excellent electron transfer ability. For example, Jing et al.[16] synthesized Fe_2O_3/graphene composites to enhance degradation ability. Zhang et al.[17] synthesized graphene oxide-Fe_2O_3 as a highly efficient heterogeneous catalyst. In our work, the former strategy has been applied to prepare hybrid photocatalysts. Based on the above analysis, the combination of Fe_2O_3 and g-C_3N_4 is expected to improve the performance in photocatalysis.

Transition metal oxide materials have outstanding properties of magnetism. Fe_2O_3, as a transition metal oxide material, was synthesized with good magnetic property in this study. In addition, g-C_3N_4 is a semiconductor material, which is beneficial for improving the performance of Fe_2O_3. From the above analysis, Fe_2O_3/g-C_3N_4 composites may possess magnetic properties when Fe_2O_3 is combined with g-C_3N_4, and our experiment further demonstrated that the composites exhibit a perfect magnetic performance. All in all, the magnetic g-C_3N_4-based composites are easy to separate from the solution after the reaction.

In this study, Fe_2O_3/g-C_3N_4 nanocomposites were synthesized by a two-step method. First, the precursor of Fe_2O_3 was prepared by a hydrothermal method. Then, the as-prepared cocoon-like Fe_2O_3 was mixed with g-C_3N_4 by a simple mixing method. The Fe_2O_3/g-C_3N_4 composites have a special magnetic property and a superior photocatalytic activity. Moreover, the Fe_2O_3/g-C_3N_4 nanocomposites can be easily separated from the treated solution by an external magnet for recycling.

EXPERIMENTAL

Sample Preparation

First, the precursor of Fe_2O_3 was prepared by a hydrothermal method: 0.27 g $FeCl_3 \cdot 6H_2O$ was dissolved in 70 mL distilled water, and then 10 mL ethylene glycol and 2 M NaOH were put into it and dispersed for 30 min in solution with magnetic stirring at room temperature. Next, the mixed solution was added into the Teflon-lined autoclaves at 200°C for 20 h. Then, the obtained precipitates were washed with distilled water and ethanol four times and the particles were dried at 60°C for 12 h and transferred to the muffle furnace at 600°C for 1 h to obtain Fe_2O_3. Second, the g-C_3N_4 powder was synthesized by heating urea up to 520°C in a muffle furnace for 2 h. Finally, the g-C_3N_4 and Fe_2O_3 were mixed in a beaker at a ratio of 3:2 and dispersed by ultrasonication at room temperature for 1 h. The precipitate was washed with distilled water and ethanol several times and then dried at 120°C for 8 h to obtain the Fe_2O_3/g-C_3N_4 composites.[18]

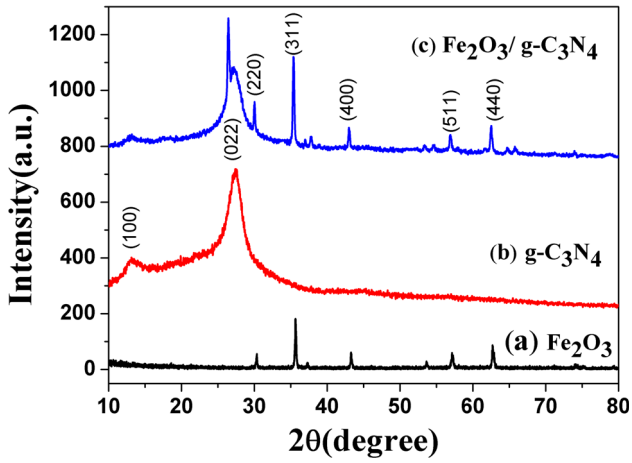

Fig. 1. XRD spectra of samples including Fe_2O_3 (a), g-C_3N_4 (b), and Fe_2O_3/g-C_3N_4 particles (c).

Characterization

The crystal phase of the samples was analyzed by x-ray diffraction (XRD) analysis using CuKa radiation at 40 kV and 20 mA with a scanning speed of 4°/min from 10° to 80°. Scanning electron microscopy (SEM) micrographs of the particles were taken with a JEM-2100SX Hitachi S-4800.The magnetic properties of the prepared samples were measured by a vibrating sample magnetometer (VSM), MicroSense EZ9. The photocatalytic activities of the synthesized samples were evaluated by degrading Rhodamine B (RhB) dye and exposure under a 300-W xenon lamp. In the experimental procedure, a 0.07-g prepared sample was added to 70 mL RhB solution (10 mg L^{-1}) in a beaker. Prior to the irradiation, the mixed solution was dispersed by ultrasonication for 30 min to establish an adsorption–desorption equilibrium. Solutions were extracted every 30 min from the beaker, and the mixed liquid was analyzed by a UV–Vis spectrometer (UV3200S; MAPADA, Shanghai, China).

RESULTS AND DISCUSSION

X-ray Diffraction Characterization

The samples were analyzed by XRD and the diffraction spectra are shown in Fig. 1. As shown in Fig. 1b, the XRD pattern of the pure g-C_3N_4 exhibits two peaks at 13.1° and 27.4°, which were matched with the (100) and (002) planes of g-C_3N_4. From Fig. 1a and c, the diffraction peaks of pure Fe_2O_3 and Fe_2O_3/g-C_3N_4 samples appear at 30.2°, 35.6°, 43.3°, 57.3°, and 62.9°, which are ascribed to the (220), (311), (400), (511), and (440) planes of Fe_2O_3, respectively (JCPDS NO. 39-1346). Furthermore, the diffraction peaks of the g-C_3N_4 can be observed after the combination with Fe_2O_3 in Fig. 1c, because Fe_2O_3 is combined on the surface of the g-C_3N_4 rather than doped into the lattice of g-C_3N_4.[3]

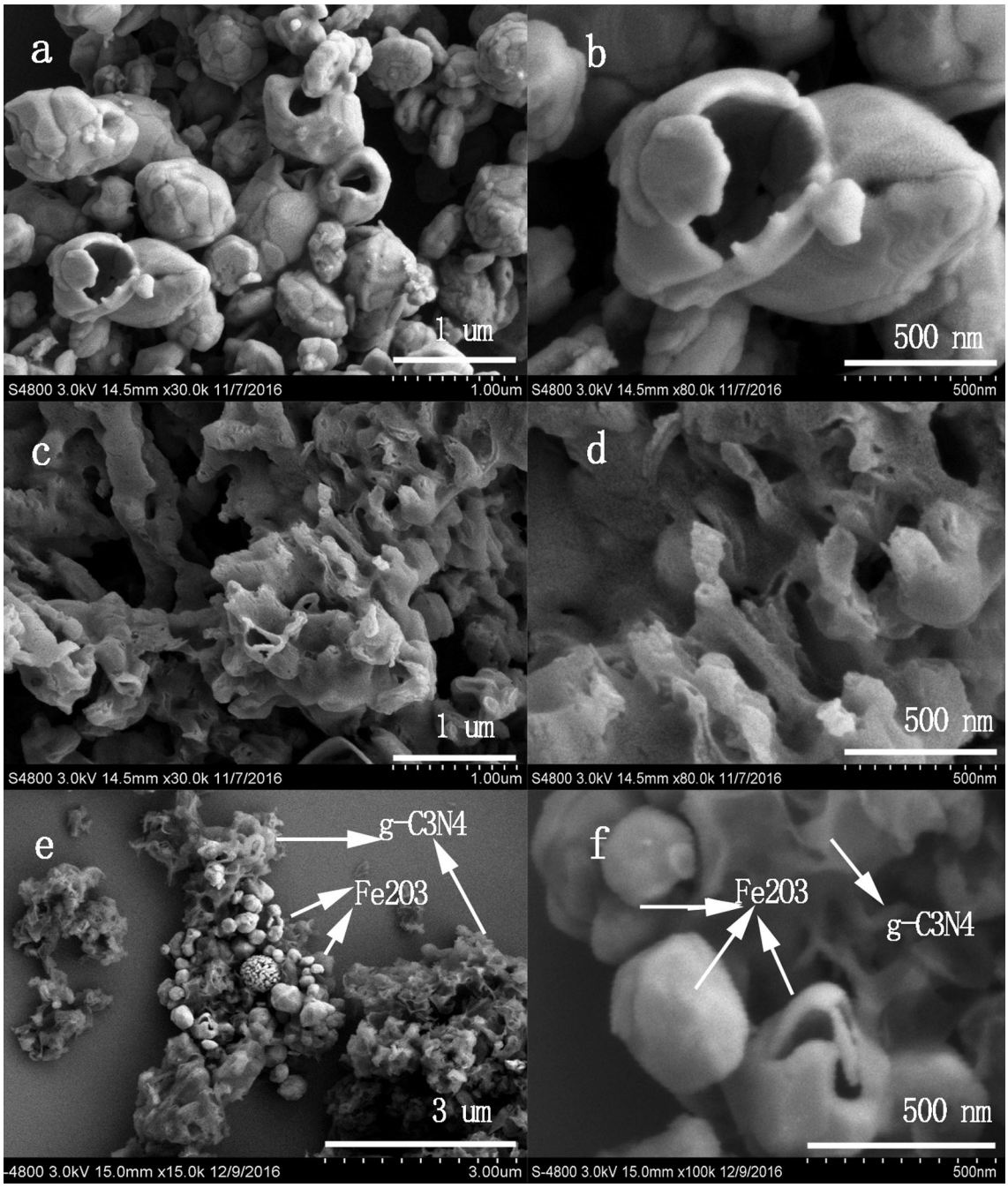

Fig. 2. SEM images of the samples including Fe_2O_3 (a, b), g-C_3N_4 (c, d), and Fe_2O_3/g-C_3N_4 particles (e, f).

Scanning Electron Microscopy Characterization

The morphology of the products are displayed in Fig. 2a–f including Fe_2O_3, g-C_3N_4 and Fe_2O_3/g-C_3N_4 nanoparticles. As illustrated in Fig. 2a and b, the Fe_2O_3 sample shows a special cocoon-like shape, and the size of the cocoon-like nanostructure is estimated to be 500 nm. Figure 2c and d shows a uniform layered morphology of the g-C_3N_4 with irregular shape and porous structure. The g-C_3N_4 also exhibits the particles aggregation including a good deal of irregular smaller crystals.[19] The Fe_2O_3 is successfully dispersed on the surface of the g-C_3N_4 with a porous nanostructure to form Fe_2O_3/g-C_3N_4 nanoparticles, which are presented in Fig. 2e and f. It is obvious that the Fe_2O_3 cocoon-like nanostructure is coated onto the layered structure of the g-C_3N_4 as shown in Fig. 2f.

Magnetic Properties

The magnetic properties of the Fe_2O_3, g-C_3N_4 and Fe_2O_3/g-C_3N_4 nanoparticles were investigated by

VSM as shown in Fig. 3. The g-C_3N_4 sample presents diamagnetism which is shown in the inset. Obviously, the saturated magnetization of Fe_2O_3 is different from the Fe_2O_3/g-C_3N_4 samples. As shown in Fig. 3, the saturation magnetization (Ms) of the Fe_2O_3 nanoparticles decreases from about 75 emu/g to 9.9 emu/g when combined with the g-C_3N_4 particles. This may be attributed to depositing on the surface of the g-C_3N_4, which has been confirmed in SEM images. In detail, the decrease of the saturation magnetization is related to the influence of the surface on the nanoparticles. The existence of diamagnetic g-C_3N_4 avoids aggregation of magnetic Fe_2O_3 nanoparticles. It may be because the Fe_2O_3 nanoparticles are dispersed by the g-C_3N_4 nanoparticles making the uniformity decrease. And it can also be contributed to the quenching of surface moments, which leads to the reduction of the magnetic moment in Fe_2O_3/g-C_3N_4 nanocomposites.[20] Furthermore, the decrease of the saturated magnetization for Fe_2O_3/g-C_3N_4 nanocomposites may also be ascribed to the fact that the presence of the ferromagnetic Fe_2O_3 molar fraction is smaller than the diamagnetic g-C_3N_4 molar fraction.[21,22] The coercivity (Hc) of Fe_2O_3 and Fe_2O_3/g-C_3N_4 samples is about 226.02 Oe and 171.14 Oe. When combining Fe_2O_3 with g-C_3N_4, the coercivity decreased with the presence of g-C_3N_4. The decrease of coercivity of the Fe_2O_3/g-C_3N_4 samples may rely on the viscosity of the nanocomposite materials. The frictional interaction between the nanoparticles of Fe_2O_3 and the polymer chain of g-C_3N_4 is related to the viscosity of the Fe_2O_3/g-C_3N_4 nanocomposites. The frictional force of the Fe_2O_3/g-C_3N_4 nanocomposites restrains the movement of the magnetic moment of the nanoparticles within the polymer matrix, which results in a decrease in the coercive force.[23–25] Furthermore, the magnetic nanoparticles are improved for decontamination processes. This is attributed to separatine the magnetic nanoparticles (Fe_2O_3 and Fe_2O_3/g-C_3N_4 particles) easily from the reaction system after RhB degradation.

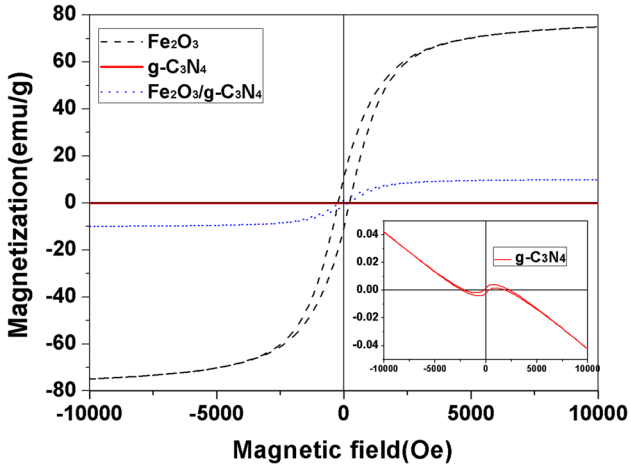

Fig. 3. Magnetization curves of the samples including Fe_2O_3, g-C_3N_4 and Fe_2O_3/g-C_3N_4 particles, and the magnetic property of g-C_3N_4 shown in the inset.

Photocatalytic Activities

The photocatalytic activities of the prepared samples were investigated via photodegradation of RhB under visible-light irradiation. As shown in Fig. 4a, the adsorption properties and photocatalytic activities were studied for the photodegradation reaction on the prepared samples including Fe_2O_3, g-C_3N_4 and Fe_2O_3/g-C_3N_4 particles. Prior to the irradiation, it can be seen that there is an adsorption–desorption equilibrium state to reach for all the samples tested. In the dark experiment, the adsorptions of RhB on the Fe_2O_3 and g-C_3N_4 samples were weaker than on the Fe_2O_3/g-C_3N_4 samples because of the interaction with each other.

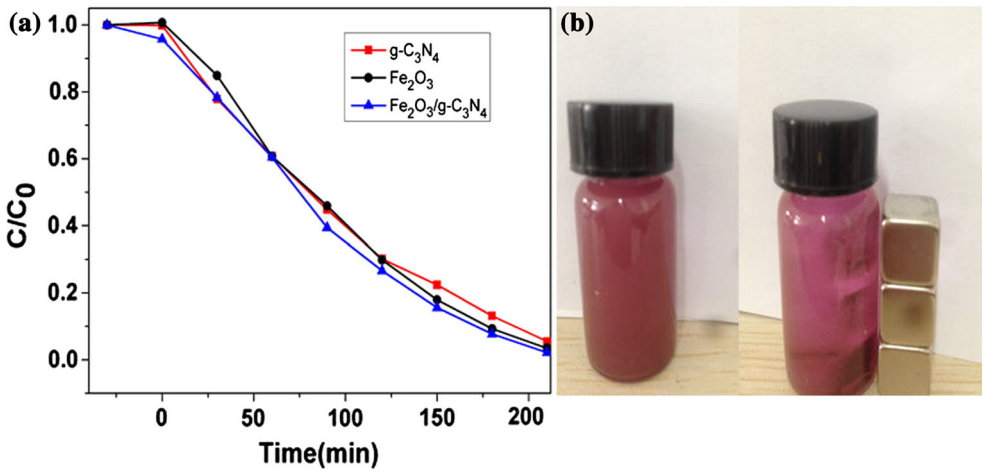

Fig. 4. The photocatalytic ability of samples including Fe_2O_3, g-C_3N_4 and Fe_2O_3/g-C_3N_4 photocatalysts (a), and of Fe_2O_3/g-C_3N_4 photocatalyst before and after magnetic separation (b).

This is attributed to the loading of the Fe_2O_3 nanoparticles on the surface ofthe Fe_2O_3/g-C_3N_4 nanocomposites. Furthermore, the specific adsorption–desorption equilibrium state of Fe_2O_3/g-C_3N_4 samples may be ascribed to the hierarchical structure, which was formed by the interaction of Fe_2O_3 and g-C_3N_4.[26,27] As shown in Fig. 4, there is a small difference between the g-C_3N_4 and Fe_2O_3/g-C_3N_4 photocatalysts before irradiation for 60 min for photocatalytic degradation reactions of RhB. However, the photocatalytic activity of Fe_2O_3/g-C_3N_4 nanocomposites is higher than that of the g-C_3N_4 photocatalyst after irradiation for 60 min, while 86.9% of RhB molecules were degraded on pure g-C_3N_4 and 92.3% of RhB molecules were degraded on Fe_2O_3/g-C_3N_4 nanocomposites after 180 min under the irradiation. It is evident that the photocatalytic capability of Fe_2O_3/g-C_3N_4 nanocomposites is superior to that of pure g-C_3N_4, and the photocatalytic degradation reactions of RhB over the Fe_2O_3 photocatalyst can be degraded by 90.8% for 180 min under irradiation. When g-C_3N_4 was introduced, the degradation rate of the Fe_2O_3/g-C_3N_4 photocatalyst increased to 92.3% for 180 min. Furthermore, the Fe_2O_3/g-C_3N_4 nanocomposites can further degrade 97.9% RhB under the visible-light irradiation for 210 min. Obviously, the photocatalytic activity of Fe_2O_3/g-C_3N_4 is higher than that of pure Fe_2O_3 and g-C_3N_4. And the photocatalytic activities of samples are connected to their compositions.[21] When combining Fe_2O_3 with g-C_3N_4, the photocatalytic activity can be affected by the interaction between them. This is attributed to the internal interaction of Fe_2O_3 and g-C_3N_4 enhancing the efficiency of charge separation and increasing the visible-light ability.[28] In addition, the magnetic Fe_2O_3/g-C_3N_4 nanocomposites could be separated from the treated solution by a magnet, as shown in Fig. 4b. In conclusion, the magnetic nanocomposites are sufficient to be magnetically separated from the solution after the photocatalytic reaction and to possess a good recycling property.

CONCLUSION

Magnetically separable nanocomposites were synthesized by a facile two-step hydrothermal method. The prepared samples were characterized by different techniques, which investigated their structures, morphology, magnetic properties, and photocatalytic activities. The Fe_2O_3 with a cocoon-like shape was surrounded by the g-C_3N_4 with uniform layered morphology. In addition, the saturated magnetization Ms of the Fe_2O_3/g-C_3N_4 nanoparticles obviously decreased in the presence of g-C_3N_4. In addition, the Fe_2O_3/g-C_3N_4 photocatalyst possesses the highest photoactivity among the prepared photocatalysts, which can enhance the efficiency of charge separation. Furthermore, the Fe_2O_3/g-C_3N_4 photocatalyst can be easily separated from the treated solution by an external magnet.

ACKNOWLEDGEMENTS

This work was financially supported by National Natural Science Foundation of China (11674001), Anhui Provincial Natural Science Foundation (1708085MA07), the Opening Project of State Key Laboratory of High-Performance Ceramics and Superfine Microstructure (SKL201607SIC), and in part by the National Natural Science Foundation of China (11174002).

REFERENCES

1. H.L. Wang, L.S. Zhang, Z.G. Chen, J.Q. Hu, S.J. Li, Z.H. Wang, J.S. Liu, and X.C. Wang, *Chem. Soc. Rev.* 43, 5234 (2014).
2. X.C. Wang, K. Maeda, A. Thomas, K. Takanabe, G. Xin, J.M. Carlsson, and K. Domen, *Nat. Mater.* 8, 76 (2009).
3. Y.G. Xu, S.Q. Huang, M. Xie, Y.P. Li, H. Xu, L.Y. Huang, Q. Zhang, and H.M. Li, *RSC Adv.* 5, 95727 (2015).
4. J.A. Singh, S.H. Overbury, N.J. Dudney, M.J. Li, and G.M. Veith, *ACS Catal.* 2, 1138 (2012).
5. S.C. Yan, Z.S. Li, and Z.G. Zou, *Langmuir* 26, 3894 (2010).
6. H. Xu, J. Yan, Y.G. Xu, Y.H. Song, H.M. Li, J.X. Xia, C.J. Huang, and H.L. Wan, *Appl. Catal. B* 129, 182 (2013).
7. S.W. Zhang, J.X. Li, M.Y. Zeng, G.X. Zhao, J.Z. Xu, W.P. Hu, and X.K. Wang, *ACS Appl. Mater. Interfaces* 5, 12735 (2013).
8. S. Ye, L.G. Qiu, Y.P. Yuan, Y.J. Zhu, J. Xia, and J.F. Zhu, *J. Mater. Chem. A* 1, 3008 (2013).
9. K. Sivula, F.L. Formal, and M. Gratzel, *Chemsuschem* 4, 432 (2011).
10. F. Shi, M.K. Tse, M.M. Pohl, A. Bruckner, and S.M. Zhang, *Angew. Chem. Int. Ed.* 46, 8866 (2007).
11. A.K. Srivastava, P. Sachan, C. Samanta, K. Mukhopadhyay, and A. Sharma, *Appl. Surf. Sci.* 288, 215 (2014).
12. Y.J. Lin, S. Zhou, S.W. Sheehan, and D.W. Wang, *J. Am. Chem. Soc.* 133, 2398 (2011).
13. B. Klahr, S. Gimenez, F. Fabregat-Santiago, T. Hamann, and J. Bisquert, *J. Am. Chem. Soc.* 134, 4294 (2012).
14. W. Wu, S.F. Zhang, X.H. Xiao, J. Zhou, F. Ren, L.L. Sun, and C.Z. Jiang *ACS Appl. Mater. Interfaces* 4, 3602 (2012).
15. Y. Liu, L. Yu, Y. Hu, C. Guo, F. Zhang, and X.W. Lou, *Nanoscale* 4, 183 (2012).
16. L.M. He, L.Q. Jing, Z.J. Li, W.T. Sun, and C. Liu, *RSC Adv.* 3, 7438 (2013).
17. S. Guo, G.K. Zhang, Y.D. Guo, and J.C. Yu, *Carbon* 60, 437 (2013).
18. Y.J. Zhang, D.K. Zhang, W.M. Guo, and S.J. Chen, *J. Alloys Compd.* 685, 84 (2016).
19. J. Theerthagiri, R.A. Senthil, A. Priya, J. Madhavan, R.J.V. Michael, and M. Ashokkumar, *RSC Adv.* 4, 38222 (2014).
20. N. Limchoowong, P. Sricharoen, Y. Areerob, P. Nuengmatcha, T. Sripakdee, S. Techawongstien, and S. Chanthai, *Food Chem.* 230, 388 (2017).
21. S.-Q. Liu, *Environ. Chem. Lett.* 10, 209 (2012).
22. W. Wu, C. Jiang, and V.A.L. Roy, *Nanoscale* 7, 38 (2015).
23. P. Jayakrishnan and M.T. Ramesan, *Polym. Bull.* 74, 3179 (2017).
24. A. Demortiere, P. Panissod, B.P. Pichon, G. Pourroy, D. Guillon, B. Donnio, and S. Begin-Colin, *Nanoscale* 3, 225 (2011).
25. W. Wu, X.H. Xiao, F. Ren, S.F. Zhang, and C.Z. Jiang, *J. Low Temp. Phys.* 168, 306 (2012).
26. Z. Jiang, D. Jiang, Z. Yan, D. Liu, K. Qian, and J. Xie, *Appl. Catal. B: Environ.* 170–171, 195 (2015).
27. S.-Z. Wu, K. Li, and W.-D. Zhang, *Appl. Surf. Sci.* 324, 324 (2015).
28. S.S. Duan, G.S. Han, Y.H. Su, X.Y. Zhang, Y.Y. Liu, X.L. Wu, and B.J. Li, *Langmuir* 32, 6272 (2016).